Research Square

Preprints are preliminary reports that have not undergone peer review. They should not be considered conclusive, used to inform clinical practice, or referenced by the media as validated information.

A Rule-Breaking Class of Planar Central Chiral Molecules in Planar Tetracoordinate Carbon Systems

Krishnan Thirumoorthy

kthirumoorthy@gmail.com

Vellore Institute of Technology https://orcid.org/0000-0003-0920-4547

Devipriya Sivadasan

Vellore Institute of Technology

Article

Keywords:

Posted Date: October 21st, 2026

DOI: https://doi.org/10.21203/rs.3.rs-11445029/v1

License: This work is licensed under a Creative Commons Attribution 4.0 International License. Read Full License

Additional Declarations: There is **NO** Competing Interest.

A Rule-Breaking Class of Planar Central Chiral Molecules in Planar Tetracoordinate Carbon Systems

Devipriya Sivadasan [1], Krishnan Thirumoorthy [1, 2]*

[1]Department of Chemistry, School of Advanced Sciences, Vellore Institute of Technology, Vellore 632014, Tamil Nadu, India.

[2]School of Computer Science and Engineering, Vellore Institute of Technology, Vellore 632014, Tamil Nadu, India.

Correspondence: Krishnan Thirumoorthy (kthirumoorthy@gmail.com & thirumoorthy.krishnan@vit.ac.in)

Abstract: Unusual bonding, stability, and potential applications of planar tetracoordinate carbon (ptC) have captivated researchers over the past five decades. Chirality has been reported in both a central carbon in a non-planar structure and in a planar geometry without a central carbon. Here, for the first time, the present work introduces the concept of planar tetracoordinate chiral carbon (ptCC) systems, in which four distinct ligands create an asymmetric center while maintaining planar tetracoordination at the carbon. This study identifies eight ptC structures that exhibit chirality and form enantiomeric pairs. The chemical bonding and stability of the ptCC structures were analyzed using the Adaptive Natural Density Partitioning, and Electron Localization Function. The aromaticity of ptCC geometries was assessed using nucleus-independent chemical shift analysis. The chirality of the ptCC systems was confirmed by examining their chiroptical properties, as evidenced by electronic circular dichroism and vibrational circular dichroism spectra. The observed chiroptical spectral features show mirror-image profiles for the enantiomeric pairs investigated. As discussed, this rule-breaking class of ptC molecules exhibits chirality at the planar central carbon. The ptCC systems investigated exhibit structural features that suggest potential utility in asymmetric catalysis and materials applications.

Introduction

Chirality denotes the intrinsic behavior of a molecule that makes it non-superimposable on its mirror image, a feature often described as molecular handedness.[1] Molecular dissymmetry of chiral molecules was first discovered by French chemist Louis Pasteur in 1848, which established the field of stereochemistry.[2] This phenomenon continues to captivate researchers because of its profound implications for biological evolution, and it has become a fundamental concept across many fields, including medicine, biology, and organic chemistry.[3] Chiral asymmetry is pervasive in nature, as we have seen in snail shells, which typically exhibit a preferred coiling direction,[4] and the rotational behavior of cyclones arises from the Coriolis effect.[5] At the molecular scale, chirality is central to life itself, and proteins are constructed from amino acids that predominantly occur in the left-handed (*L*) configuration, whereas the sugars essential to biological systems are mainly found in the right-handed (*D*) form.[6] Chirality in chemistry can arise either from central chirality, where a chiral center (carbon atom bonded to

four different substituents) is present, or from planar chirality, which occurs without a chiral center.[7] In the case of pillar-like structured molecules, planar chirality arises from the specific way the ring components are linked. These systems are generally symmetrical macrocyclic structures composed of multiple polycyclic aromatic panels connected by linear linkages. The spatial arrangement and restricted rotation of these panels in relation to the macrocyclic framework give rise to planar chirality.[7] Such geometries may generate multiple stereoisomeric forms, commonly described as *pS* and *pR* configurations. These structures are well known for their notable catalytic behavior and different chiroptical properties.[8]

Central chirality arises when a central carbon atom is bonded to four different substituents, prompting van't Hoff[9] to explore carbon's tetrahedral geometry and reach the same conclusion as Le Bel,[10] who proposed that a carbon atom bonded to four substituents adopts a tetrahedral geometry. It became a foundational breakthrough in organic chemistry, enabling a better understanding of carbon stereochemistry.[11]

For more than a century, the possibility of unusual carbon geometries has intrigued chemists, and the concept of planar tetracoordinate carbon (ptC) was first proposed by Monkhorst in 1968.[12] Further, in 1970, Hoffmann and co-workers proposed, on theoretical grounds, a new class of molecules featuring ptC,[13] in contrast to the tetrahedral model.[14] Schleyer and coworkers carried out theoretical investigations, demonstrating that such geometries could be stabilized by two general strategies. The first is an electronic strategy,[15] in which the carbon atom is bonded to neighboring atoms that serve as strong σ-donors and π-acceptors, helping to maintain the required electronic structure for planarity. The second is a mechanical strategy,[15] in which the ptC structure is stabilized by geometric constraints, such as embedding it within cages, cyclic frameworks, or coordination environments involving transition metals, thereby enforcing a planar arrangement.[16] The inclusion of σ-donor and π-acceptor elements such as aluminum,[17,18] boron,[19] beryllium,[20] can significantly stabilize the lone pair in the p_z orbital of ptC structures. The ligands like B, Be, and Al donate their electron density through a σ bond, and their empty p orbital receives non-bonding lone pairs in the ptC through delocalization. Experimental studies[21,22] have reported ptC in various metal complexes via synthesis, providing strong evidence for unconventional geometries, such as planar tetracoordinate systems. This planar tetracoordination has been observed not only in carbon but also in other elements, such as boron,[23,24] iron,[25] and phosphorus,[26] as well as for fluorine[27] and oxygen.[28] Beyond chemical curiosities, ptC geometries are extended to investigate their potential as catalysts.[29] Recent studies reported that the ptC geometry of $CAl_3MgH_2^-$ system can catalyze the hydrogenation of alkyne[30] and conversion of acetone to isopropyl alcohol.[31]

Chiral catalysts hold an uncontested place in catalysis because of their chiral-selective applications, and they can be sorted into organometallic,[32–34] organocatalytic[35,36] and biocatalytic[37] catalysis. Beyond tetrahedral geometries, the possibility of chirality without a chiral centre is explored in square planar complexes with chiral and achiral ligands.[38,39] In 2000, Fu reported that planar chiral complexes can function with relatively low energy barriers, making them comparable with conventional catalysts such as

N-heterocyclic carbenes.[40] Although these geometries have attracted considerable attention, central chirality in planar molecules has remained unexplored to date.

In this work, we have introduced, for the first time, potential enantiomeric pairs of planar tetracoordinate chiral carbon (ptCC) structures and analyzed their chemical bonding, stability and chiroptical properties. **Figure 1** shows 2D representations of the geometries of the investigated ptCC systems and their enantiomers, along with their absolute configurations. These planar chiral ptC molecules could be potential candidates for chiral-selective catalytic applications.

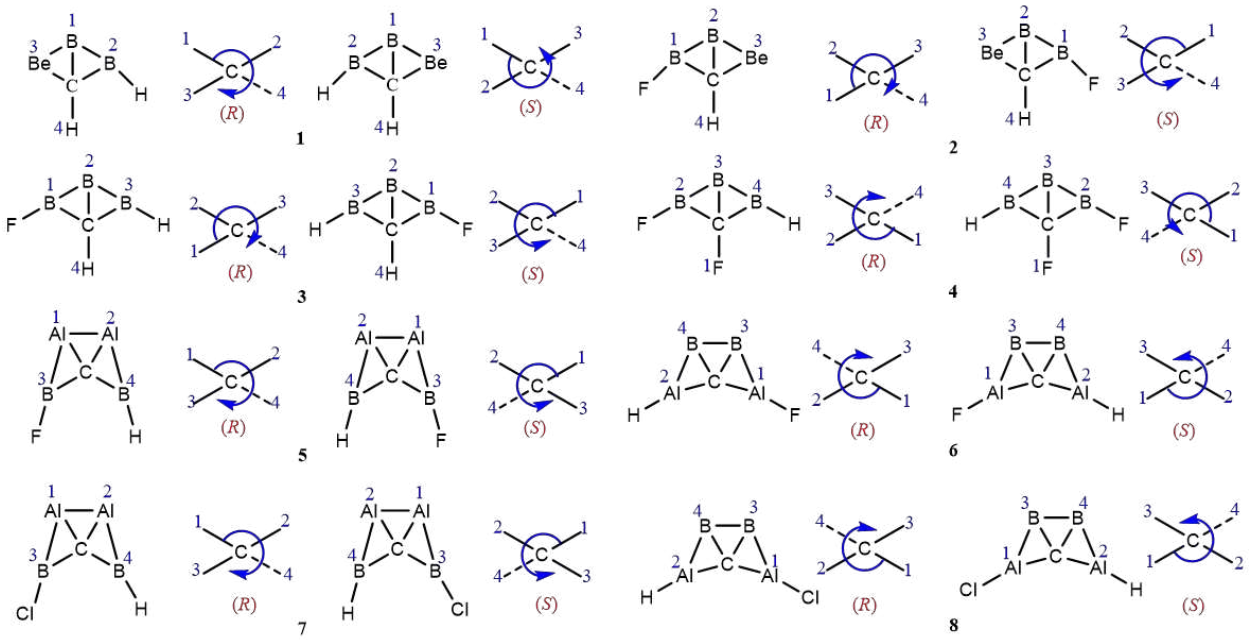

Figure 1. 2D representation of ptCC systems with their absolute configuration.

Computational methods

All the ptCC geometries were optimized at ωB97XD[41]/aug-cc-pVTZ[42,43], MP2[44]/aug-cc-pVTZ, and CCSD[45]/aug-cc-pVTZ theoretical levels. Harmonic vibrational frequencies were calculated to determine whether the obtained ptCC geometries correspond to minima on the potential energy surface. Single-point energy calculations were carried out at CCSD(T)[46]/aug-cc-pVTZ//CCSD/aug-cc-pVTZ level. Natural bond orbital analysis was carried out to explore atomic charges and Wiberg bond indices[47] through the NBO 3.1 program[48] implemented in the Gaussian 16 package. Adaptive natural density partitioning (AdNDP) analysis[49,50] was performed to confirm their chemical bonding patterns and stability of the investigated ptCC systems. Nucleus-independent chemical shift analysis (NICS)[51] was carried out using the Gaussian 16 package. Electron localization function (ELF),[52] plots were generated with the Multiwfn

software[53] to visualize the electron density and the localization and delocalization of electrons. To analyze the chiroptical properties, Electronic circular dichroism (ECD) calculations were carried out using time-dependent density functional theory (TD-DFT)[54–56] at the ωB97XD[41]/aug-cc-pVTZ[42,43] level of theory, and the solvent effect of methanol was incorporated using the polarizable continuum model (PCM).[57] The calculated excitation energies, oscillator strengths, and rotatory strength values obtained from the TD-DFT calculations were processed using the Multiwfn software[53] to simulate the ECD spectra[58] for predicting chiroptical properties of the investigated ptCC enantiomers. Vibrational circular dichroism (VCD)[59] calculations were performed at the ωB97XD/aug-cc-pVTZ level of theory to assess the chiroptical properties. All quantum-chemical calculations were performed using the Gaussian 16 package.[60]

Results and Discussion

This work investigated chirality in ptC by generating possible neutral ptCC geometries based on chemical intuition in the singlet state and evaluating them with quantum-chemical calculations. The geometry of ptCC enantiomers optimized at the CCSD/aug-cc-pVTZ level of theory is shown in **Figure 2**, and the corresponding geometries obtained at the ωB97XD/aug-cc-pVTZ and MP2/aug-cc-pVTZ levels of theory are shown in **Figure S1** and **S2**, respectively. The single-point calculations were obtained at the CCSD(T)/aug-cc-pVTZ//CCSD/aug-cc-pVTZ level. Harmonic vibrational spectral analysis shows that all geometries have no imaginary frequencies and are minima on the potential energy surface. Based on the literature, incorporating σ-donors and π-acceptor ligands into a small three-membered ring will help overcome steric effects and stabilize the ptCC structure.[15] Due to the asymmetric environment created by the ligands, the identified geometries exhibit central-planar chirality in ptC systems. The enantiomers of **1** and **2** consist of six atoms, with the central carbon atom surrounded by two B atoms, one Be atom, and 1 H atom. Both B and Be contribute to the stability of the ptC structure by donating σ-electron density and receiving electron density through π bonds.[15,61] All the other geometries from **3R** to **8S** have seven atoms. The ptCC structures **3R** and **3S** were generated from **2R** and **2S** by replacing the Be atom with B-H. This geometry is surrounded by three B atoms and stabilized by electronic interactions. From **3R** and **3S**, the H atom bonded to C is displaced by the electronegative atom F to form **4R** and **4S**. In this geometry, F aids stability alongside B. The ptCC structures **5R** to **8S** have the central carbon atom surrounded by ligands such as Al and B atoms. Among these, the enantiomeric pair **5** and **6** consist of isomers with F atoms attached to B and Al, respectively. Similarly, enantiomeric pair **7** and **8** are isomers with a Cl atom attached. In these isomers, two Al atoms and two B atoms together stabilize the ptC geometry. The bond lengths of C-B agree with the standard bond lengths in all eight geometries, but in **4R** and **4S**, the bond length C-B is longer due to the influence of the F atom bonded to C.[62] Dipole moment helps the experimentalist to identify them spectroscopically. The investigated ptCC geometries with a non-zero dipole moment are likely to be detected in rotational spectroscopy.

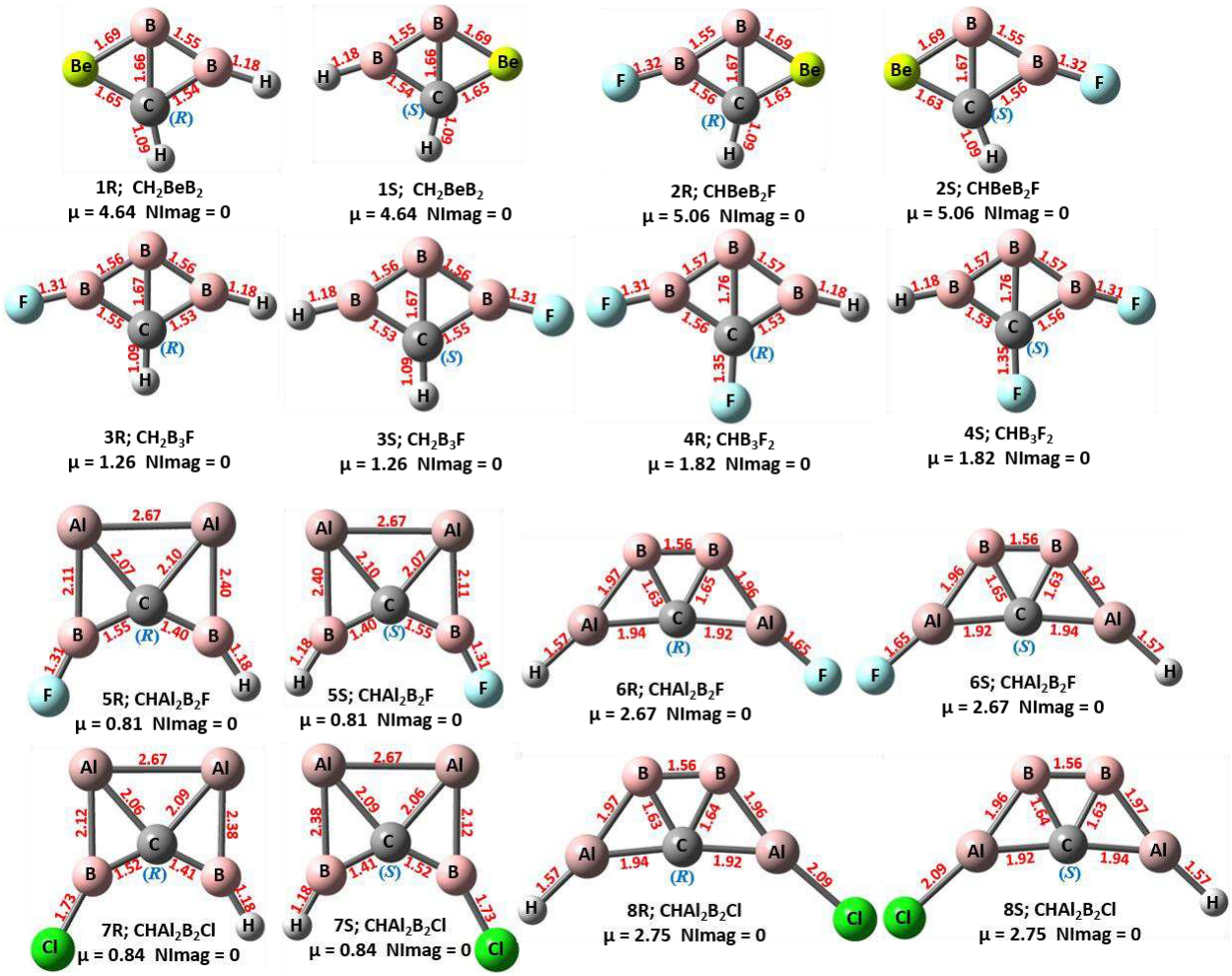

Figure 2. Optimized geometries of ptCC systems with their bond lengths in Å, absolute configurations in (blue), chemical formula, dipole moments (in Debye), and the number of imaginary frequencies (NImag) calculated at the CCSD/aug-cc-pVTZ level of theory.

All ptCC geometries contain a chiral carbon; although the carbon is bonded to the same types of atoms, differences in substituent environments create an asymmetric environment. Energies for all optimized geometries of ptCC systems at the ωB97XD/aug-cc-pVTZ, MP2/aug-cc-pVTZ and CCSD/aug-cc-pVTZ levels of theory are listed in **Tables S1**, **S2**, and **S3**, respectively. Single-point energies of CCSD(T)/aug-cc-pVTZ//CCSD/aug-cc-pVTZ levels are listed in **Table S4**. The total energy of ptCC systems at all four levels of theory and the number of imaginary frequencies are listed in **Table 1**.

Table 1. Chemical formulae, total energies (E+ZPVE), and the number of imaginary frequencies (NImag) of ptCC systems calculated at different levels.

Chemical Formula	ptCC Systems	Total energy (a.u)				NImag
		ωB97XD/aug-cc-pVTZ	MP2/aug-cc-pVTZ	CCSD/aug-cc-pVTZ	CCSD(T)/aug-cc-pVTZ//CCSD/aug-cc-pVTZ	
CH_2BeB_2	1R	-103.602	-103.303	-103.322	-103.348	0
	1S	-103.602	-103.303	-103.322	-103.348	0
$CHBeB_2F$	2R	-202.917	-202.509	-202.522	-202.555	0
	2S	-202.917	-202.509	-202.522	-202.555	0
CH_2B_3F	3R	-213.677	-213.257	-213.275	-213.309	0
	3S	-213.677	-213.257	-213.275	-213.309	0
CHB_3F_2	4R	-312.904	-312.369	-312.383	-312.427	0
	4S	-312.904	-312.369	-312.383	-312.427	0
$CHAl_2B_2F$*	5R	-673.086	-671.88	-671.891	-671.937	0
	5S	-673.086	-671.88	-671.891	-671.937	0
	6R	-673.056	-671.849	-671.863	-671.904	0
	6S	-673.056	-671.849	-671.863	-671.904	0
$CHAl_2B_2Cl$*	7R	-1033.434	-1031.84	-1031.866	-1031.915	0
	7S	-1033.434	-1031.84	-1031.866	-1031.915	0
	8R	-1033.418	-1031.82	-1031.850	-1031.893	0
	8S	-1033.418	-1031.82	-1031.850	-1031.893	0

Structural isomers are marked with an asterisk

All the optimized geometries of ptCC systems show positive imaginary frequencies. The calculated energies of the enantiomeric pairs are isoenergetic. In addition, the corresponding structural parameters (bond lengths and bond angles) and dipole moments are the same, confirming the equivalent energetics and structural properties of enantiomers.

Structural parameter

The bond lengths between planar tetracoordinate carbon and the neighboring atoms obtained from the optimized geometries of the ptCC systems using the four different computational methods were analyzed and summarized in **Table S5**. In enantiomeric pairs **1**, **2**, **3**, and **4**, ptC bonded with B, Be, F, and H as neighboring atoms, but the remaining geometries of enantiomers in which the ptC were formed bond with

B and Al as their neighboring atoms. The obtained bond lengths agree closely with the standard bond lengths,[62] revealing the tetracoordination of carbon and its neighbouring atoms.

Structural isomers

Among these ptCC systems, two sets of structural isomers were identified (denoted by an asterisk in **Table 1**), and their relative energies were compared and listed in **Table 2**. Enantiomeric geometries **5** and **6** differ in atom connectivity, and their relative energies are 18.38 kcal mol^{-1} at the MP2 level and 17.71 kcal mol^{-1} at the ωB97XD level. The relative energy obtained at the CCSD level is 16.64 kcal mol^{-1}. Similarly, **7** and **8** differ in structure, and their energy difference is 14.48 kcal mol-1 at the MP2 level, 9.78 kcal mol-1 at the ωB97XD level, and 9.62 kcal mol^{-1} at the CCSD level. The relative-energy trend holds across different levels of theory and does not change the relative stability of isomeric pairs. For geometries **5** and **6**, the relative energy difference ranges from 17 to 20 kcal mol^{-1}, and geometry **5** is more stable than **6**. Similarly, for geometries **7** and **8**, the relative energy difference ranges from 10 to 15 kcal mol^{-1}, and geometry **7** is more stable than **8**. This work also investigates their bonding patterns and structural stability.

Table 2. Total relative energies (ΔE; in kcal mol^{-1}), ZPVE-corrected relative energies (ΔE+ZPVE; in kcal mol^{-1}) of ptCC systems calculated at MP2/aug-cc-pVTZ, ωB97XD/aug-cc-pVTZ, CCSD/aug-cc-pVTZ and CCSD(T)/aug-cc-pVTZ//CCSD/aug-cc-pVTZ levels of theory.

ptCC systems	Chemical Formula	Absolute configuration	ΔE+ZPVE (kcal/mol)			ΔE (kcal/mol)			
			ωB97XD/aug-cc-pVTZ	MP2/aug-cc-pVTZ	CCSD/aug-cc-pVTZ	ωB97XD/aug-cc-pVTZ	MP2/aug-cc-pVTZ	CCSD/aug-cc-pVTZ	CCSD(T)/aug-cc-pVTZ//CCSD/aug-cc-pVTZ
5	$CHAl_2B_2F$	R	0	0	0	0	0	0	0
		S							
6		R	17.70	18.38	16.64	18.71	19.89	17.58	20.32
		S							
7	$CHAl_2B_2Cl$	R	0	0	0	0	0	0	0
		S							
8		R	9.78	14.48	9.62	10.51	15.70	10.15	13.74
		S							

NBO analysis

Natural bond orbital (NBO) analysis provides information on the charge-transfer nature of σ-donating and π-accepting substituents, as well as the electron density around the carbon atom and its four substituents. **Figure 3** shows the natural atomic charges (NAC) obtained from the NBO analysis. The central ptC carbon atom in all 8 enantiomeric pairs shows a negative charge, whereas the neighboring atoms like Al, Be, and B show positive charge, which confirms that the central carbon received electron density from the surrounding atoms, such as σ-donors and π-acceptor ligands, to stabilize the planar tetracoordinate geometry. The hydrogen atom retains a positive charge only when it is connected to a carbon atom. In geometries where boron is attached to both carbon and beryllium bear a negative charge due to its contribution to aromaticity. The natural atomic charges and the Wiberg bond indices are listed in **Table S6** and **Table S7**, respectively. WBI values show the bonding nature of the carbon and its neighboring atoms. The $WBI_{C\text{-}B}$ is 0.9-1.25, which shows a strong covalent single bond. The $WBI_{C\text{-}Al}$ (0.32-0.45) is relatively small, indicating weak covalent bonds. Similarly, the $WBI_{C\text{-}Be}$ (0.17-0.60) is relatively small, indicating weak covalent bonds. The $WBI_{C\text{-}F}$ is 0.86, which shows that the C-F bond is mainly covalent.

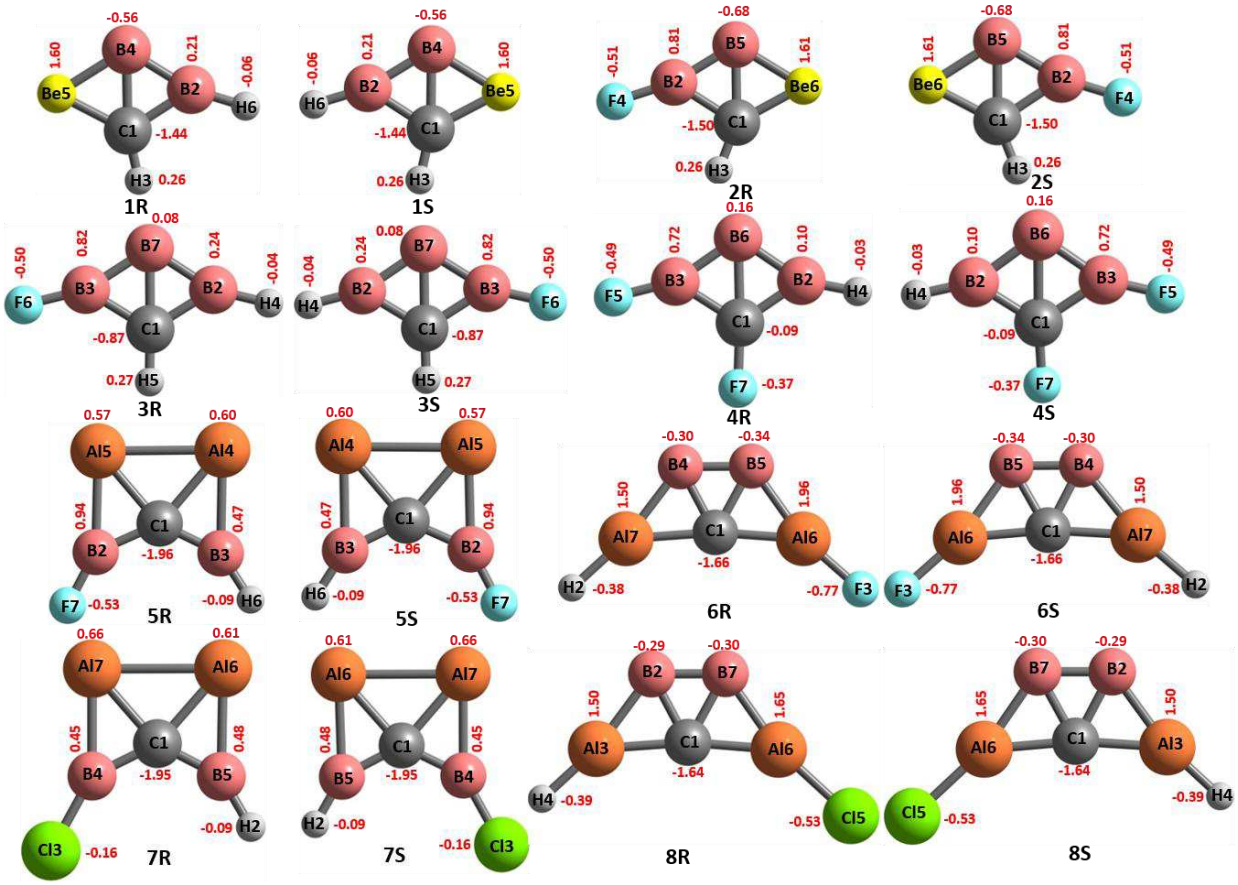

Figure 3. The natural atomic charges (red colour) for ptCC molecules at MP2/aug-cc-pVTZ level of theory

Topology analysis

The electron localization function (ELF) is widely used to determine electron localization, identify bond pairs, lone pairs, and delocalized electrons. The color-filled ELF plots of ptCC systems are shown in **Figure 4**, revealing interactions between the central carbon and its neighboring atoms through the localization and delocalization of electron density. Electron density is measured on a scale ranging from 0 to 1. The values near 1 indicate electron localization, while those near 0.2 indicate delocalization of electron density. In these colored ELF plots, the interaction between the central carbon and the neighboring atoms is shown as reddish-orange in color, which is evident for the strong covalent bond. Electron delocalization around the central carbon and its neighbors is illustrated as a green-to-blue ring. These plots reveal that the electron density is delocalized throughout the system. Thus, electron delocalization promotes the structural stability of the investigated enantiomeric pairs.

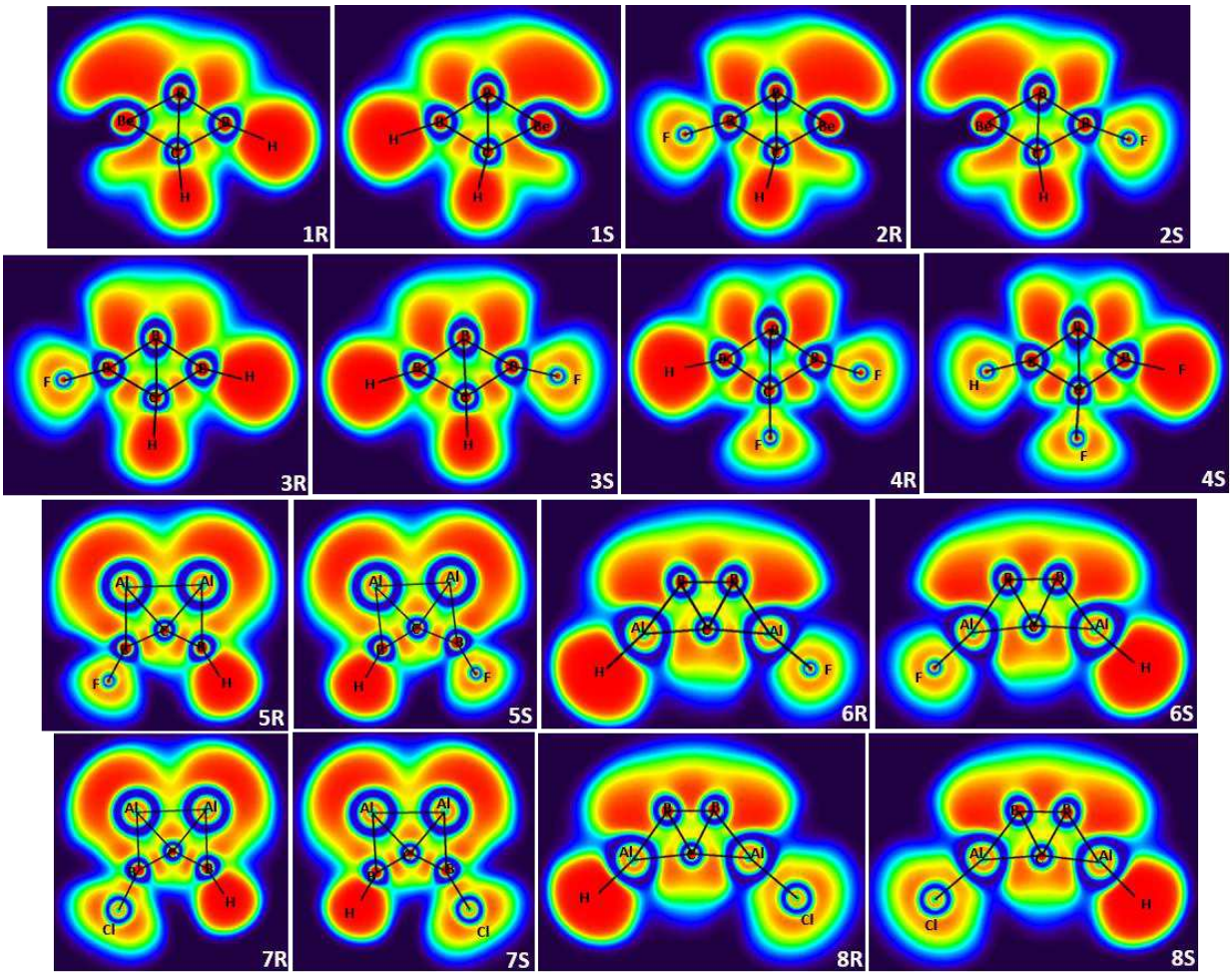

Figure 4. Color-filled maps of the ELF of ptCC systems at the MP2/aug-cc-pVTZ level of theory.

AdNDP analysis

Adaptive Natural Density Partitioning (AdNDP) analysis has been performed to assess the bonding nature of the obtained ptCC geometries. **Figure 5** illustrates the delocalized π-electron density around the ptCC geometries, with occupancy number (ON). Geometries **1R** to **4S** depict 4c-2e π bonds because one of the neighboring atoms to the central carbon is hydrogen or fluorine, as it is not involved in π delocalization. All other geometries, like **5R** to **8S,** depict 5c-2e π bonds. Geometries **1R** to **5S** have an ON range of 2.00|e|, indicating strong delocalization of electron density. Enantiomeric geometries **6** and **8** show an ON range of 1.88|e| and 1.87|e|, respectively. Geometry **7** shows the 5c-2e π bonds with an ON range of 1.91|e|. AdNDP patterns show the delocalization of lone pairs of the ptCC with π-accepting ligands. These bonding patterns confirm the π-aromaticity that helps maintain the stability of planar, tetracoordinate chiral carbon systems.

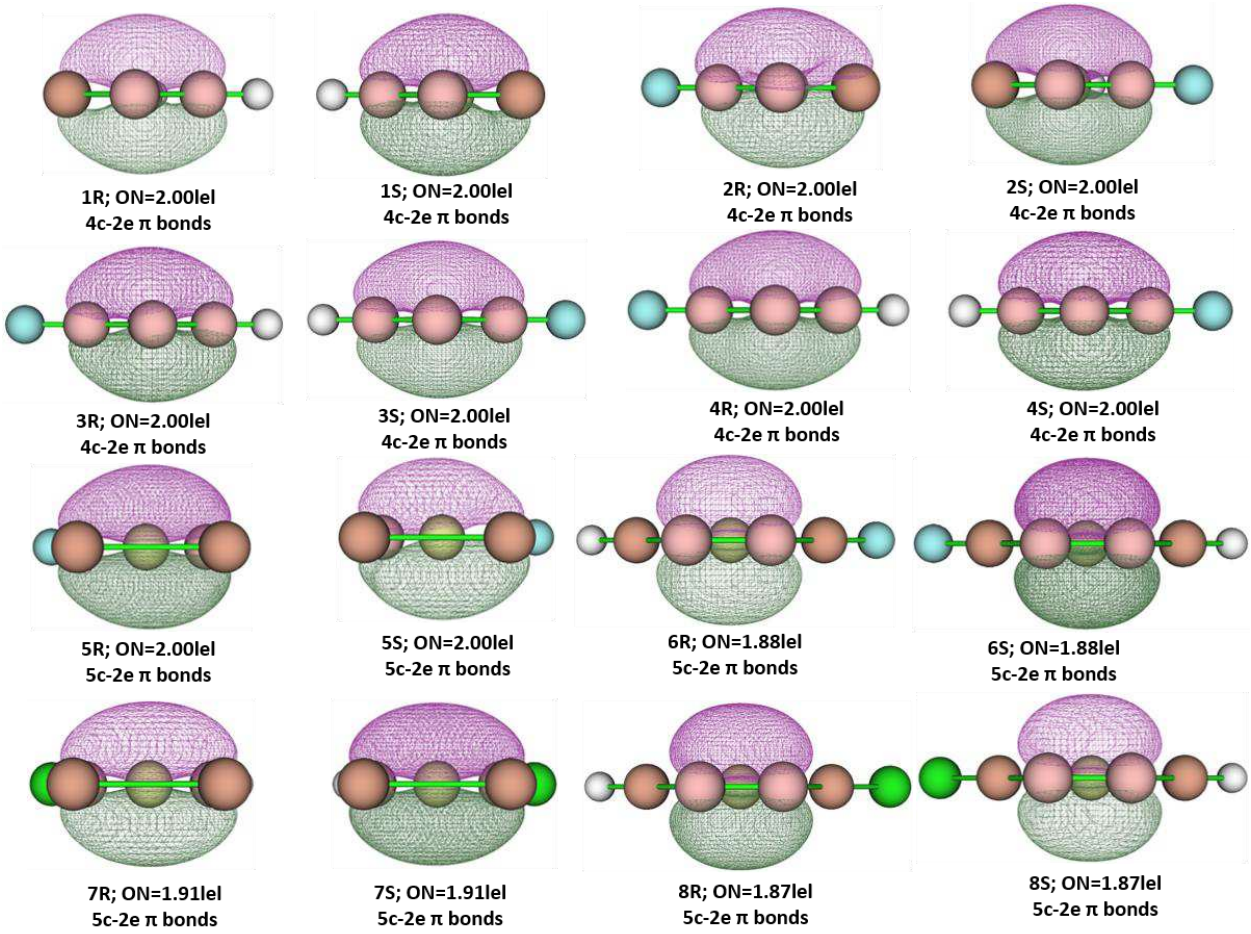

Figure 5. AdNDP patterns of nc-2e π bonds with occupation numbers (ONs) of ptCC molecules at MP2/aug-cc-pVTZ level of theory.

Nucleus-independent chemical shift analysis

Aromaticity of ptCC geometries is analyzed theoretically using Nucleus-Independent Chemical Shift (NICS), and its values were calculated from the magnetic properties of all three-membered rings in ptCC geometries, as illustrated in **Figure 6**. Negative NICS values indicate the aromatic nature of the geometries. NICS(0) values indicate σ-aromaticity, whereas NICS(1) values indicate π-aromaticity. NICS analysis confirmed double aromaticity and agrees with the AdNDP analysis, indicating that delocalisation of σ and π bonds stabilizes the ptCC geometries.

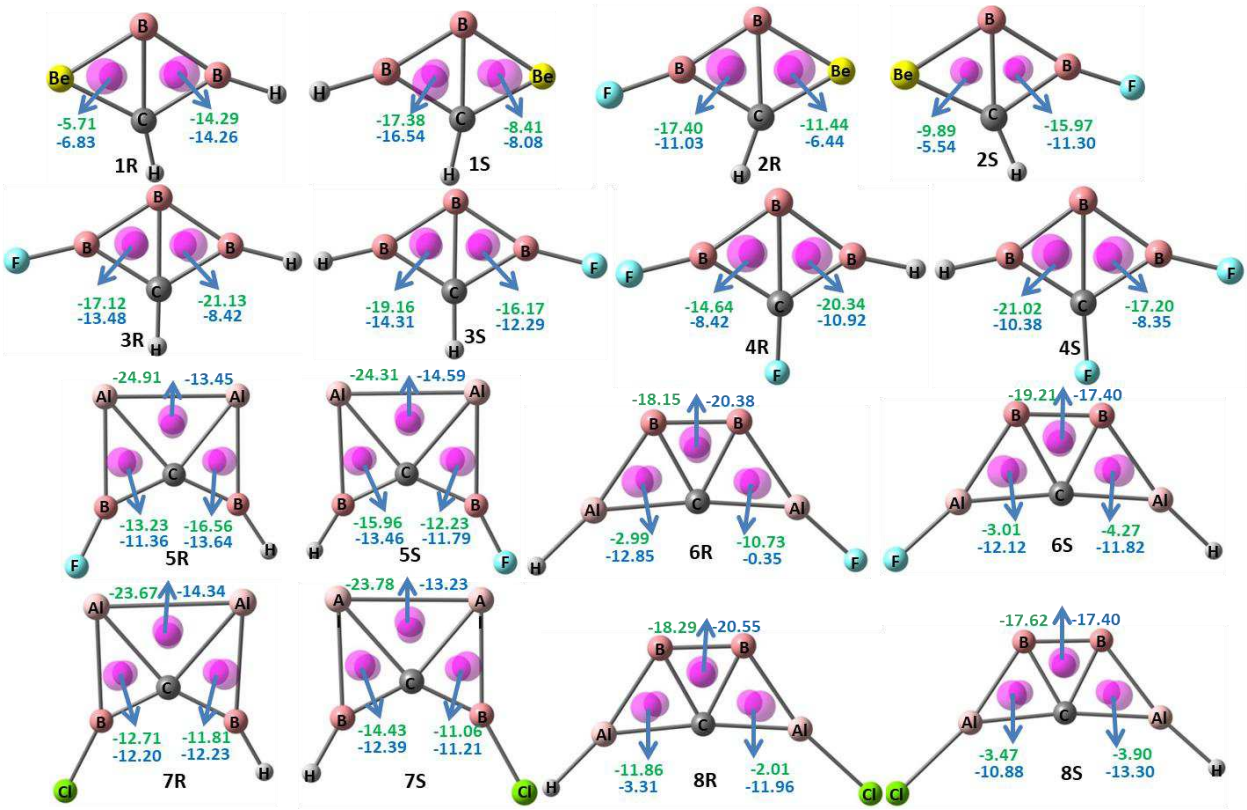

Figure 6. Nucleus-independent chemical shifts (NICSs; in ppm) of ptCC geometries. The green and blue values indicate NICS(0) and NICS(1), respectively, at the MP2/aug-cc-pVTZ level of theory.

Chiroptical analysis

Chiroptical analyses were carried out to investigate the chiral nature of the theoretically identified ptCC geometries, and their chiroptical properties were studied through electronic circular dichroism (ECD) and vibrational circular dichroism (VCD) calculations at the ωB97X-D/aug-cc-pVTZ level of theory. Chiroptical spectroscopies are usually very sensitive to molecular handedness because they arise from the differential absorption of left- and right-circularly polarised light. While ECD provides chiral responses associated with electronic transitions, VCD provides complementary information from vibrational

transitions. Combined ECD and VCD analysis enables examination of the chiral behaviour of ptCC geometries at both electronic and vibrational levels.

Electronic circular dichroism (ECD)

Electronic circular dichroism has become one of the most significant chiroptical techniques to investigate molecular chirality and the stereochemical relationship of enantiomers, and it gives information regarding molecular chirality through differential absorption of left- and right-circularly polarized light during electronic transitions. ECD spectra of planar tetracoordinate chiral carbon geometries were calculated using time-dependent density functional theory at the ωB97X-D/aug-cc-pVTZ level of theory, and the data were extracted from the Multiwfn software. TDDFT provides the energies, oscillator strengths and rotational strengths of electronic excitation of chiral molecules. The ECD spectra are plotted against wavelength (λ) in nm on the X-axis and the differential molar extinction coefficient (arbitrary units) on the Y-axis. **Figure 7** shows the calculated ECD spectra of the R- and S-configured enantiomers in the ptCC geometry. Enantiomers are mirror images, so their spectra have opposite signs but the same magnitude. In ptCC geometry **1**, the R-configured geometry shows a strong positive Cotton effect at 185 nm, whereas the S-configured geometry shows a strong negative Cotton effect at 185 nm. In ptCC geometry **2**, the 2S enantiomer shows a positive Cotton effect and the 2R enantiomer shows a negative Cotton effect at 300 nm. All other enantiomers show positive and negative Cotton effects in the 150-200 nm range. The ECD spectra of the investigated ptCC enantiomers show positive and negative peaks of equal magnitude but opposite sign. This ECD pattern is expected for enantiomers of ptCC geometries, which are mirror images and chiral.

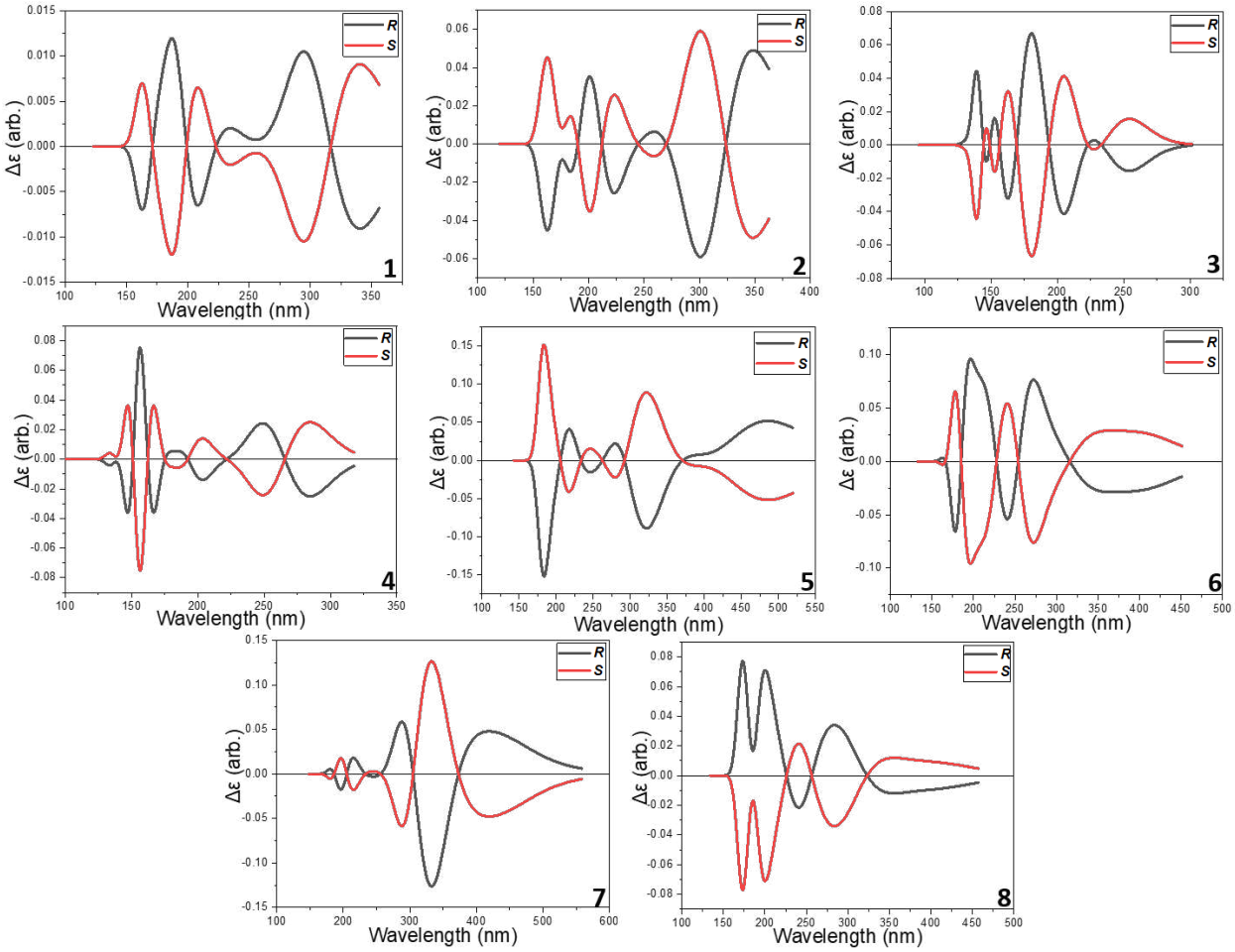

Figure 7. ECD spectra of enantiomers of ptCC molecules obtained at the ωB97XD/aug-cc-pVTZ level of theory**.**

Vibrational circular dichroism (VCD)

To investigate the chiral nature and enantiomeric relationship of the theoretically identified ptCC geometries, vibrational circular dichroism (VCD) spectra were computed at the ωB97X-D/aug-cc-pVTZ level of theory, and data were extracted from Multiwfn software. VCD technique is an extension of ECD spectra, and it can be used to analyze the absolute configurations of chiral compounds, and it measures the difference in the absorbance of left- and right- circularly polarized light in the infrared region. VCD is highly sensitive to the three-dimensional arrangement of atoms and is widely used for stereochemical and conformational analysis. The VCD spectra are plotted against wavenumber in cm^{-1} on the X-axis and the differential molar extinction coefficient (arbitrary units) on the Y-axis. The VCD spectra of ptCC geometries are illustrated in **Figure 8**. The VCD spectra of the ptCC enantiomers show that both

enantiomers have the same peak intensity and magnitude but opposite signs, indicating they are mirror images of each other and chiral.

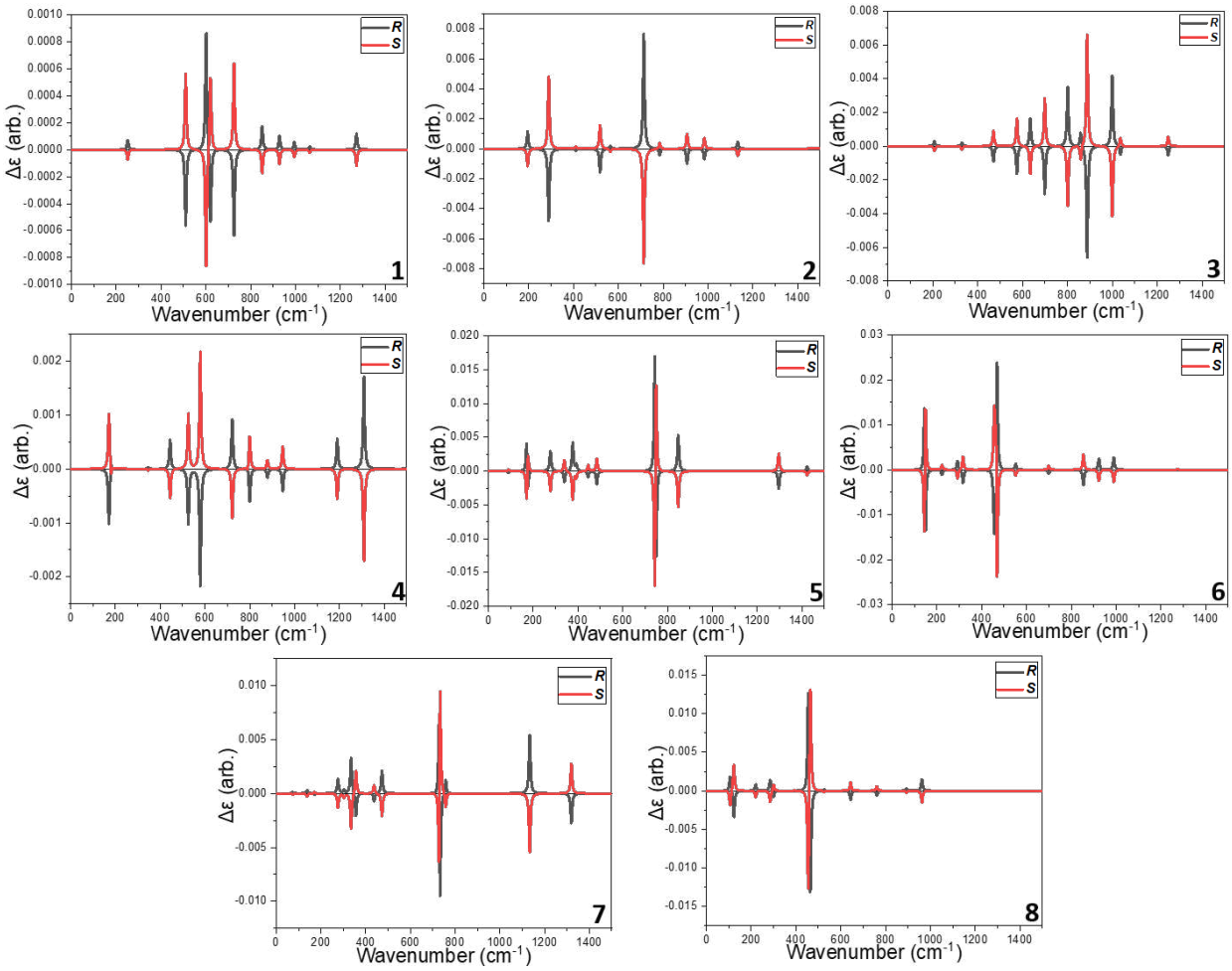

Figure 8. VCD spectra of ptCC geometries obtained at ωB97XD/aug-cc-pVTZ level of theory

Question on point group

The unconventional planar tetracoordinate chiral carbon (ptCC) systems identified in this work show distinct structural arrangements. Conventional chiral carbon systems fall under central chirality, in which a stereocenter is connected to four different substituents in a tetrahedral structure with the C_1 point group, reflecting the absence of an improper axis of symmetry. Molecules that exhibit planar chirality (without a chiral centre) have the C_1 point group due to their structural arrangement. In contrast, other categories of chirality, such as axial and helical forms, have the C_2 point group but remain chiral because rotation is restricted. In planar tetracoordinate chiral carbon systems, this becomes rule-breaking because the central carbon retains its stereocenter while simultaneously being part of an unconventional planar

environment. The combination of planar tetracoordinate carbon systems and the central chirality forced the ptCC systems to possess C_s point group. This work shows that central chirality can emerge from non-tetrahedral geometry, thus breaking the conventional requirement for chirality-related symmetry elements.

Conclusion

The concept of planar central chirality is introduced for the first time in ptC geometries. In this work, 8 enantiomeric pairs of ptCC systems were identified for the first time using ωB97XD/aug-cc-pVTZ, MP2/aug-cc-pVTZ, and CCSD/aug-cc-pVTZ levels of theory. All geometries have no imaginary frequencies, confirming they are true minima. Single-point calculations were performed at the CCSD (T)/aug-cc-pVTZ//CCSD/aug-cc-pVTZ level of theory. Natural atomic charges and Wiberg bond indices obtained from NBO analysis determine the nature of the central carbon atom and its bonding interactions with surrounding atoms. The AdNDP analysis illustrates multi-centre bonding in the ptCC geometries, providing strong evidence for their stability due to electron delocalization on the central carbon and its neighboring atoms. NICS analysis confirmed the σ- and π-aromaticity of ptCC geometries and supported the σ- and π-delocalization observed in the AdNDP analysis. The ELF plots revealed the localization of the electron pair, the delocalization of the multi-centred bond, and its stability. Chiroptical analyses such as ECD and VCD were carried out for the ptCC systems, and their spectra show that these enantiomers are mirror images of each other. The investigated systems provide a novel structural framework for examining how molecular symmetry, geometry, and stereogenicity interrelate when the conventional tetrahedral rule is broken. This work paves the way for experimentalists to probe planar central chirality more deeply for chiral-selective catalytic applications.

Data availability

The optimized geometries of ptCC systems at the ωB97XD/aug-cc-pVTZ and MP2/aug-cc-pVTZ levels, the energies of geometries optimized at the ωB97XD/aug-cc-pVTZ, MP2/aug-cc-pVTZ and CCSD/aug-cc-pVTZ levels, total energies obtained in the CCSD(T)/aug-cc-pVTZ//CCSD/aug-cc-pVTZ level, structural parameters such as bond lengths, the natural atomic charges, Wiberg bond indices, and Cartesian coordinates of ptCC systems are provided in the supporting information.

References

1. Cahn, R. S., Ingold, C. & Prelog, V. Specification of Molecular Chirality. *Angew. Chem. Int. Ed* **5**, 385–415 (1966).

2. Pasteur, L. Memoire sur la relation qui peut exister entre la forme cristalline et la composition chimique, et sur la cause de la polarisationrotatoire. *Comptes. rendus* **26**, 535–538 (1848).

3. Feringa, B. L. & van Delden, R. A. Absolute Asymmetric Synthesis: The Origin, Control, and Amplification of Chirality. *Angew. Chem. Int. Ed.* **38**, 3418–3438 (1999).

4. Schilthuizen, M. & Davison, A. The convoluted evolution of snail chirality. *Naturwissenschaften* **92**, 504–515 (2005).

5. Arteaga, O. *et al.* Flow Effects in Supramolecular Chirality. *Isr. J. Chem.* **51**, 1007–1016 (2011).

6. Forbes, K. A. Twisted light and twisted matter: the photonic frontier of chirality. *Photonics Res.* **14**, B193 (2026).

7. Kato, K., Fa, S. & Ogoshi, T. Alignment and Dynamic Inversion of Planar Chirality in Pillar[n]arenes. *Angew. Chem. Int. Ed.* **62**, (2023).

8. Lopez, R. & Palomo, C. Planar Chirality: A Mine for Catalysis and Structure Discovery. *Angew. Chem. Int. Ed.* **61**, (2022).

9. van't Hoff & Jacobus Hendrikus. A suggestion looking to the extension into space of the structural formulas at present used in chemistry. *Arch. Neerl. Sci. Exact. Nat* **9**, 445–454 (1874).

10. Le Bel & Joseph Achille. On the relations which exist between the atomic formulas of organic compounds and the rotatory power of their solutions. *Bull. Soc. chim. Fr* **22**, 337–347 (1874).

11. Keese, R. Carbon Flatland: Planar Tetracoordinate Carbon and Fenestranes. *Chem. Rev.* **106**, 4787–4808 (2006).

12. Monkhorst, H. J. Activation energy for interconversion of enantiomers containing an asymmetric carbon atom without breaking bonds. *Chem. Commun.* **18**, 1111-1112 (1968).

13. Hoffmann, R., Alder, R. W. & Wilcox, C. F. Planar tetracoordinate carbon. *J. Am. Chem. Soc.* **92**, 4992–4993 (1970).

14. Hoffmann, R. The theoretical design of novel stabilized systems. *Pure Appl. Chem.* **28**, 181–194 (1971).

15. Collins, J. B. *et al.* Stabilization of planar tetracoordinate carbon. *J. Am. Chem. Soc.* **98**, 5419–5427 (1976).

16. von Ragué Schleyer, P. & Boldyrev, A. I. A new, general strategy for achieving planar tetracoordinate geometries for carbon and other second row periodic elements. *J. Chem. Soc., Chem. Commun.* 1536–1538 (1991).

17. Boldyrev, A. I. *et al.* Experimental Observation of Pentaatomic Tetracoordinate Planar Si-and Ge-Containing Molecules: MAl_4^- and MAl_4^-. *J. Chem. Soc. Chem. Commun* **39**, 30 (2000).

18. Malhan, A. H. & Thirumoorthy, K. Global minimum and a heap of low-lying isomers with planar tetracoordinate carbon in the $CAl_3MgH_2^-$ system. *Phys. Chem. Chem. Phys*. **26**, 3804–3809 (2024).

19. Heine, T. & Merino, G. What Is the Maximum Coordination Number in a Planar Structure? *Angew. Chem. Int. Ed.* **51**, 4275–4276 (2012).

20. Xiao, B., Ding, Y. & Sun, C. Beryllium and boron decoration forms planar tetracoordinate carbon strips at the edge of graphene nanoribbons. *Phys. Chem. Chem. Phys.* **13**, 2732–2737 (2011).

21. Cotton, F. A. & Millar, M. The probable existence of a triple bond between two vanadium atoms. *J. Am. Chem. Soc.* **99**, 7886–7891 (1977).

22. Buchwald, S. L., Lucas, E. A. & Davis, W. M. A bimetallic zirconium complex containing an in-plane bridging aromatic ring. *J. Am. Chem. Soc.* **111**, 397–398 (1989).

23. Khatun, M. *et al.* $BAl_4Mg^{-/0/+}$: Global Minima with a Planar Tetracoordinate or Hypercoordinate Boron Atom. *Atoms* **9**, 89 (2021).

24. Chakraborty, B. & Chattaraj, P. K. Exploring the Possibility of a Planar Tetracoordinate Boron in BXY_3 (X = B, Al, Ga; Y = C, Si, Ge) Clusters: A Theoretical Study. *J. Comput. Chem.* **46**, e27525 (2025).

25. Shajan, S., Thirunavukkarsu, K., Chandrasekaran, V., Thimmakondu, V. S. & Thirumoorthy, K. $FeC_4H_2^{2+}$ Encompassing Planar Tetracoordinate Iron: Structure and Bonding Patterns. *Atoms* **12**, 11 (2024).

26. Driess, M., Aust, J., Merz, K. & van Wüllen, C. van't Hoff-Le Bel Stranger: Formation of a Phosphonium Cation with a Planar Tetracoordinate Phosphorus Atom. *Angew. Chem. Int. Ed.* **38**, 3677–3680 (1999).

27. Sarmah, K., Bai, L., Guo, J. & Guha, A. K. Planar Tetracoordinate Fluorine in Binary Clusters. *ChemPhysChem* **26**, e202500154 (2025).

28. Sarmah, K. *et al.* Noble gas decorated planar tetracoordinate oxygen. *Phys. Chem. Chem. Phys.* **27**, 10923–10926 (2025).

29. Zhang, M., Gu, J. & Zhao, Y. Au^1 Complexes with Planar Tetracoordinate Carbon and Their Catalytic Activity for the Rearrangement of Allylic Acetates: A Computational Study. *ACS Omega* **10**, 12514–12521 (2025).

30. Malhan, A. H. & Thirumoorthy, K. Catalytic hydrogenation of alkyne with planar tetracoordinate carbon in $CAl_3MgH_2^-$ system. *Front. Chem.* **13**, 1672968 (2025).

31. Malhan, A. H. & Thirumoorthy, K. Catalytic hydrogenation of acetone to isopropyl alcohol with $CAl_3MgH_2^-$ containing planar tetracoordinate carbon. *Front. Chem.* **13**, 1750798 (2026).

32. Knowles, W. S. & Sabacky, M. J. Catalytic asymmetric hydrogenation employing a soluble, optically active, rhodium complex. *Chem. Commun.* **28**, 1445-1446 (1968).

33. Miyashita, A. *et al.* Synthesis of 2,2'-bis(diphenylphosphino)-1,1'-binaphthyl (BINAP), an atropisomeric chiral bis(triaryl)phosphine, and its use in the rhodium(I)-catalyzed asymmetric hydrogenation of. alpha.-(acylamino)acrylic acids. *J. Am. Chem. Soc.* **102**, 7932–7934 (1980).

34. Katsuki, T. & Sharpless, K. B. The first practical method for asymmetric epoxidation. *J. Am. Chem. Soc.* **102**, 5974–5976 (1980).

35. List, B., Lerner, R. A. & Barbas, C. F. Proline-Catalyzed Direct Asymmetric Aldol Reactions. *J. Am. Chem. Soc.* **122**, 2395–2396 (2000).

36. Ahrendt, K. A., Borths, C. J. & MacMillan, D. W. C. New Strategies for Organic Catalysis: The First Highly Enantioselective Organocatalytic Diels−Alder Reaction. *J. Am. Chem. Soc.* **122**, 4243–4244 (2000).

37. Chen, K. & Arnold, F. H. Tuning the activity of an enzyme for unusual environments: sequential random mutagenesis of subtilisin E for catalysis in dimethylformamide. *Proceedings of the National Academy of Sciences* **90**, 5618–5622 (1993).

38. Fujita, S. Chirality and Stereogenicity of Square-Planar Complexes. *Helv. Chim. Acta* **85**, 2440–2457 (2002).

39. Biagini, M. C., Ferrari, M., Lanfranchi, M., Marchiò, L. & Pellinghelli, M. A. Chirality in mononuclear square planar complexes. *J. Chem. Soc., Dalton Trans.* **28**, 1575–1580 (1999).

40. Fu, G. C. Enantioselective Nucleophilic Catalysis with "Planar-Chiral" Heterocycles. *Acc. Chem. Res.* **33**, 412–420 (2000).

41. Chai, J. Da & Head-Gordon, M. Long-range corrected hybrid density functionals with damped atom-atom dispersion corrections. *Phys. Chem. Chem. Phys.***10**, 6615–6620 (2008).

42. Kendall, R. A., Dunning, T. H. & Harrison, R. J. Electron affinities of the first-row atoms revisited. Systematic basis sets and wave functions. *J. Chem. Phys.* **96**, 6796–6806 (1992).

43. Dunning, T. H. Gaussian basis sets for use in correlated molecular calculations. I. The atoms boron through neon and hydrogen. *J. Chem. Phys.* **90**, 1007–1023 (1989).

44. Moller, C. & Plesset, M. S. Note on an Approximation Treatment for Many-Electron Systems. *Phys. Rev* **46**, (1934).

45. Purvis III, G. D. & Bartlett, R. J. A full coupled-cluster singles and doubles model: The inclusion of disconnected triples. *J. Chem. Phys.* **76**, 1910–1918 (1982).

46. Raghavachari, K., Trucks, G. W., Pople, J. A. & Head-Gordon, M. A fifth-order perturbation comparison of electron correlation theories. *Chem. Phys. Lett.* **157**, 479–483 (1989).

47. Wiberg, K. B. Application of the pople-santry-segal CNDO method to the cyclopropylcarbinyl and cyclobutyl cation and to bicyclobutane. *Tetrahedron* **24**, 1083–1096 (1968).

48. Reed, A. E., Weinstock, R. B. & Weinhold, F. Natural population analysis. *J. Chem. Phys.* **83**, 735–746 (1985).

49. Tkachenko, N. V. & Boldyrev, A. I. Chemical bonding analysis of excited states using the adaptive natural density partitioning method. *Phys. Chem. Chem. Phys.* **21**, 9590–9596 (2019).

50. Zubarev, D. Y. & Boldyrev, A. I. "Developing paradigms of chemical bonding: Adaptive natural density partitioning. *Phys. Chem. Chem. Phys.* **10**, 5207–5217 (2008).

51. Schleyer, P. von R., Maerker, C., Dransfeld, A., Jiao, H. & van Eikema Hommes, N. J. R. Nucleus-Independent Chemical Shifts: A Simple and Efficient Aromaticity Probe. *J. Am. Chem. Soc.* **118**, 6317–6318 (1996).

52. Becke, A. D. & Edgecombe, K. E. A simple measure of electron localization in atomic and molecular systems. *J. Chem. Phys.* **92**, 5397–5403 (1990).

53. Lu, T. & Chen, F. Multiwfn: A multifunctional wavefunction analyzer. *J. Comput. Chem.* **33**, 580–592 (2012).

54. Autschbach, J., Nitsch-Velasquez, L. & Rudolph, M. Time-dependent density functional response theory for electronic chiroptical properties of chiral molecules. *Electronic and magnetic properties of chiral molecules and supramolecular architectures* **298**, 1–98 (2010).

55. Chong, D. P. Time-dependent density functional response theory for molecules. *Recent advances in density functional methods* **1**, 155–192 (1995).

56. Runge, E. & Gross, E. K. U. Density-Functional Theory for Time-Dependent Systems. *Phys. Rev. Lett.* **52**, 997–1000 (1984).

57. Scalmani, G. *et al.* Geometries and properties of excited states in the gas phase and in solution: Theory and application of a time-dependent density functional theory polarizable continuum model. *J. Chem. Phys.* **124**, (2006).

58. Stephens, P. J. & Harada, N. ECD cotton effect approximated by the Gaussian curve and other methods. *Chirality* **22**, 229–233 (2010).

59. Stephens, P. J. Theory of vibrational circular dichroism. *J. Phys. Chem.* **89**, 748–752 (2002).

60. M. J. Frisch *et al.* Gaussian 16, Revision. Preprint at (2016).

61. Wang, Z.-X., Zhang, C.-G., Chen, Z. & Schleyer, P. von R. Planar Tetracoordinate Carbon Species Involving Beryllium Substituents. *Inorg. Chem.* **47**, 1332–1336 (2008).

62. Johnson & Russell, D. NIST Computational Chemistry Comparison and Benchmark Database, NIST Standard Reference Database Number 101. *National Institute of Standards and Technology* Preprint at https://cccbdb.nist.gov/ (2022).

Acknowledgements

We gratefully acknowledge the computational facility provided by the Vellore Institute of Technology, Vellore, for carrying out this work. DS expresses gratitude for a fellowship named “Savitribai Jyotirao Phule Single Girl Child Fellowship (SJSGC) 2022 – 2023” (F.No.82-7/2022(SA-III)) provided by the University Grants Commission (UGC), New Delhi, India.

Author Contributions

Conceptualization DS and KT; investigation, data curation, visualization, and writing the original draft, DS; manuscript review, editing, and supervision, KT.

Competing interests

The authors declare no competing interests.

Supplementary Files

This is a list of supplementary files associated with this preprint. Click to download.

- 01TOYDeviNaturesi.docx